Supplementary Information

Supplementary Materials and Methods

Bacterial strains

We transformed YFP and DsRed labelled (1) strains of *P. aeruginosa* strain PA01 with plasmid Rms149 (2) by electroporation (3) using a Gene Pulser apparatus (Bio-Rad). Transformants were selected on Luria-Bertani (LB) (Fisher Scientific, NJ, USA) agar plates containing 200 μg/ml streptomycin. Plasmid transformation was confirmed by PCR (see Supplementary Experimental Procedures) using GoTaq green Mastermix (Promega, Madison, WI, USA) and by plasmid extraction using QIAprep Spin Miniprep (Qiagen, Inc., Chatworth, California, USA). Minimum inhibitory concentration (MIC) assays were performed in triplicate by agar dilution (4) (Table S1).

Rms149 is a clinical, non-conjugative, plasmid (Rms149) that confers resistance to an aminoglycoside (streptomycin), which is adenylated in the cytoplasm, and a β-lactam (carbenicillin), which is thought to be hydrolysed both in the periplasm and extracellularly. Unpublished data shows the aminoglycoside resistance locus is expressed more strongly than that of the β-lactamase (San Millan pers. comm.). The cross protection seen for the β-lactamase (but not aminoglycoside resistance), therefore, is not explained by increased gene expression in the former.

Liquid competitions

To test for cross-protection we investigated whether susceptible plasmid-free strains had a higher survival rate in the presence of resistant plasmid-bearing strains than alone. Strains were competed in increasing concentrations of antibiotic. Pre-cultures of the strains were incubated at 37 °C with 250 RPM shaking overnight in 3 ml of LB broth (Fisher Scientific, NJ, USA). Pre-cultures were diluted in 3 ml of fresh LB broth to an OD_{600} of 0.05 and incubated at the same conditions for 2 hours. Cultures of the strains were then mixed at a ratio of 1:1 in phosphate buffered saline (PBS) with an OD_{600} of 0.3. This was diluted 10-fold in PBS and 1 μl was added per well in a 96 well plate, in triplicate. Wells contained a final total volume of 200 μl LB broth with the following antibiotic concentrations: streptomycin; 1, 2, 4, 8 μg/ml and carbenicillin; 3, 6, 12, 24 μg/ml, which were chosen as sub-MIC values, and a no-antibiotic control for every competition. Competitions were run for 12 hours overnight at the ambient temperature of the lab (20 °C) at 250 RPM. Competitions were diluted 10^5-fold and 50 μl of each was added to a plate using glass beads to count colony forming units (C.F.U.), using

fluorescence to differentiate cells labelled with YFP. The number of cells in the inoculum was also measured in the same way.

Liquid competitions were also performed over 16 hours and set up in the same way without antibiotic. In order to most accurately measure the cost of the plasmid, cells from these competitions were counted using flow cytometry (5).

Competitions on agar

To investigate the conditions required for protection of the susceptible strain by a β-lactamase producing strain we performed the same competitions on solid agar plates. These were set up in the same way as liquid competitions. The resulting 1:1 mixtures were diluted by a tenth in PBS. 1 µl of this mixture was added per agar plate in a single central drop. Plates contained 25 ml 1 x LB Miller agar (40 g/l; 15 g/l of which is agar) and the following antibiotic concentrations: streptomycin; 2, 4, 8 µg/ml and carbenicillin; 6, 12, 24 µg/ml which were chosen as sub-MIC values in addition to a no antibiotic control for every competition. Initial ratios were calculated by plating 50 µl of a 10^{-6} dilution of the inocula on LB agar plates. These were incubated overnight at 37 °C so C.F.U. could be counted. Competition plates were left at 20 °C and imaged on a stereoscope daily for 6 days. On day 7 the colonies were scraped from the agar and suspended in 1 ml PBS, diluted 10^6 and 10^5-fold and plated out to count C.F.U, using fluorescence to differentiate cells labelled with YFP.

The fitness was determined using the following formula (6):

$$susceptible\ fitness = \frac{\ln\left(\frac{N_{suceptible,final}}{N_{susceptible,initial}}\right)}{\ln\left(\frac{N_{resistant,final}}{N_{resistant,initial}}\right)}$$

Where $N_{susceptible,\ initial}$ and $N_{susceptible,\ final}$ are the numbers of susceptible cells before and after the competition and $N_{resistant,\ initial}$ and $N_{resistant,\ final}$ are the numbers of resistant cells before and after the competition.

Manipulating spatial structure with inoculum density

We wished to determine the role of increasing spatial structure in colonies on susceptible fitness. To do this, structuring was created in the colony by varying the number of cells in the initial inoculum (7). The strains were set up as described above and then this 1:1 mixture was diluted 10-fold, 100-fold, and 1000-fold in PBS. Each of these dilutions was used to inoculate colonies by adding 1 µl to plates

containing either no antibiotic or 12 μg/ml carbenicillin. A 10^5-fold dilution of the initial mixture was plated out so initial ratios could be calculated from C.F.U. Plates were left at 20 ◦C and imaged on an Axio Zoom. V16 microscope (Zeiss) daily for 6 days. Half of the plates were mixed daily after imaging, using an inoculation loop (8). On the seventh day the colonies were scraped and suspended in 1 ml PBS, diluted 10^6-fold and 50 μl was plated out with glass beads to count C.F.U.

Microscopy

The Axio Zoom.V16 microscope (Zeiss) under the PlanApo Z 0.5X objective and the associated Zen Blue software was used to carry out fluorescence microscopy imaging. These colonies were imaged while still growing on the agar plate and these images were taken at 3.5X. For confocal imaging colonies were cut out of the agar plate and placed on a slide. Confocal laser scanning microscopy (CLSM) imaging was carried out with the LSM 700 laser scanning microscope (Zeiss) under the 50X objective using Zen Black software.

Aspect Ratio Experiments

We suspected cell length was driving the increase in fitness on carbenicillin. To investigate this further, susceptible and resistant cells were competed on no antibiotic and on 12 μg/ml carbenicillin, this being the concentration at which we had previously seen a cross-protective effect. Colonies were set up as previously described, as competitions on agar plates, and imaged destructively, at 40X using confocal microscopy, in triplicate, on days 0, 1, 2, 3 and 4. 1 μl of PBS was added to the edge of the colony to disperse cells so they could be counted by analysis of the image with open source FIJI software (9). The aspect ratio was assessed using the cell counting function.

Time-lapse microscopy

Colonies were inoculated in the same way as solid competitions. Cultures were allowed to grow for 10 hours at 20 ◦C. Then the colony and surrounding agar were cut out of the plate and mounted on a glass-bottomed petri dish for fluorescence imaging, using a 64X objective under oil emersion.

Statistical Analysis

Statistical analyses were carried out in R (10). An ANOVA was used unless otherwise stated; please see the Supplementary Experimental Procedures for further details. Error bars show standard error. Solid and liquid competition experiments were performed using all colour combinations to allow for different costs associated with the colour markers. For these experiments (Figures 1 and 2) the mean and standard error of two experiments, each with n = 6 for co-cultures and n = 3 for monocultures, are shown. The differences between colour markers were not significant in the solid competition experiments, hence later experiments were performed using just one colour combination and show the mean and standard deviation of two experiments with n = 3 (Figure 4).

Individual-based modelling of cell interactions at the colony edge

We ran colony growth simulations to help understand the role of cell shape in the enrichment of antibiotic-susceptible (S) cells at the colony edge during growth in the presence of the resistant strain (R), on carbenicillin. We used an individual-based computer model, based on the open source software, CellModeller 4 (11, 12), which is described in more detail later in the Supplementary Information provided (Figure S6).

In our model, sections of the colony edge are represented using collections of bacterial cells (Figures 6 and S6). Each cell is a rigid, capsule (spherocylinder) with unique index i, fixed radius r, variable segment length l_i, position $p_i = \left(p_x, p_y, p_z\right)_i^{\mathsf{T}}$ and orientation $\hat{a}_i = \left(a_x, a_y, a_z\right)_i^{\mathsf{T}}$. Capsules increase in volume V_i exponentially by elongating along their principal axes, dividing lengthways into two identical daughter cells once they double in volume. The range of aspect ratios $AR = 1 + l / 2r$ adopted during the cell cycle is controlled by changing the cell birth volume, V_0. R- and S-type capsules are set to have mean aspect ratios of 3.3 and 6.1 respectively; these parameters are drawn directly from the cell aspect ratio measurements described in this study (Figure 5A).

To represent resource competition, each cell's intrinsic growth rate is determined by the local concentration u of two non-interacting solutes, Oxygen (O) and another nutrient (N), e.g. a limiting carbon source. A cell's volume V_i increases in time t according to the equation

$$\frac{dV_i}{dt} = \mu_{max}\left(\frac{u_O(p_i)}{u_O(p_i) + K_O}\right)\left(\frac{u_N(p_i)}{u_N(p_i) + K_N}\right)V_i,$$

where K_O and K_N are saturation constants for Oxygen and nutrient uptake respectively, and μ_{max} represents the maximum solute uptake rate. All cells share the same μ_{max}, irrespective of their

morphology. $u_O(p_i)$ and $u_N(p_i)$ correspond to local Oxygen and nutrient concentrations, evaluated at the cell's centroid p_i; the fields u_O and u_N are approximated using the reaction-diffusion equations

$$D_O \nabla^2 u_O = \rho \gamma_O \mu_{max} \left(\frac{u_O}{u_O + K_O}\right)\left(\frac{u_N}{u_N + K_N}\right)\varphi(p_1 \dots p_n),$$

$$D_N \nabla^2 u_N = \rho \gamma_N \mu_{max} \left(\frac{u_O}{u_O + K_O}\right)\left(\frac{u_N}{u_N + K_N}\right)\varphi(p_1 \dots p_n),$$

where D_O, D_N and γ_O, γ_N represent solute diffusivities and substrate biomass yields for the two solutes respectively, and ρ corresponds to the cell biomass density. The scalar field $\varphi(p_1 \dots p_n)$, describes the spatial variation in cell volume fraction, computed from the cell configuration $p_1 \dots p_n$. Each simulation timestep, solute fields are computed by solving this equation in non-dimensional form using the FEniCS finite element library. Oxygen and nutrient diffuse into the domain from above and below respectively (Figure S6). Following the cell growth phase, cell configurations are returned to mechanical equilibrium using an energy minimisation algorithm (11). For simplicity, active cell motility is not included, such that only growth and cell-cell collisions cause cell movement. Mechanical boundaries at the sides and base of the domain are imposed to represent repulsive forces from the cells around and behind the edge section, and from the agar surface below it.

We used our model to grow 100 µm sections of the colony edge from 1:1 mixtures of R and S cells. Simulations were initiated by randomly placing 20 cells of each type in the area defined by $0 < x \leq 5$ µm, $0 < x \leq 100$ µm, representing the leading edge of the colony as it enters the simulation domain. Cells were then allowed to grow and divide so that the colony edge propagated in the radial (x) direction, reaching an average colony volume of 1.043 x 10^3 µm^3 (approximately 6,500 cells) after 56h. A summary of the variables and coefficients used in our model is available later in the Supplementary Experimental Procedures.

Individual-based modelling of growth in colony and planktonic environments

We used a modified version of our individual-based modelling framework to explore the effect of growing in colony and planktonic environments on fitness. Here, as with previous models (13, 14), cells are all approximately spherical instead of rod-shaped, and cellular growth is controlled by a single limiting solute. Vertical 2D colony slices were grown from 1:1 mixtures of labelled capsule cells (denoted A and B), placed randomly on the base of a 300 µm-wide box. Cells of type A were

programmed to grow exponentially at rate μ_A, whereas cells of type B grew faster at rate $\mu_B > \mu_A$, representing intrinsic differences in cell growth rate. Both cell types were given the same shape, with a birth aspect ratio of 1.1. To simplify the description of cell-solute interactions, we omitted the nutrient field from the model (corresponding to the limit u_N >> K_N), so that cell growth was made dependent on the concentration of oxygen only:

$$\frac{dV_X}{dt} = \mu_X \left(\frac{u_O}{u_O + K_O}\right) V_X, \qquad X = A, B,$$

$$D_u \nabla^2 u_O = \rho\gamma \left(\frac{u_O}{u_O + K_O}\right) [\mu_A \phi_A + \mu_B \phi_B],$$

where ϕ_A, ϕ_B represent the local volume fractions of type A and B cells respectively; other model variables have the same meanings and values as before.

We carried out simulations using values of μ_A equal to 95 or 90% of μ_B, equal to μ_O as before. In each case, the colony was fed with either a plentiful ($u_{O,0} = 500\text{x}10^{-3}$ kgm^{-3}) or a poor Oxygen supply ($u_{O,0} = 5\text{x}10^{-3}$ kgm^{-3}), representing the perfusion conditions present in liquid or solid cultures respectively. In each case, simulations were terminated once the total cell population reached a maximum value of approximately 7.5 x 10^3 cells.

In Figure S4B, we quantify this effect using boxplots of the relative cell fitness

$$\frac{\omega_B}{\omega_A} = \log\left(\frac{N_{B,final}}{N_{B,initial}}\right) / \log\left(\frac{N_{A,final}}{N_{A,initial}}\right),$$

for each case, where $N_{X,initial}$ and $N_{X,final}$ correspond to the initial and final populations of each cell type $X = A, B$.

Supplementary Figures

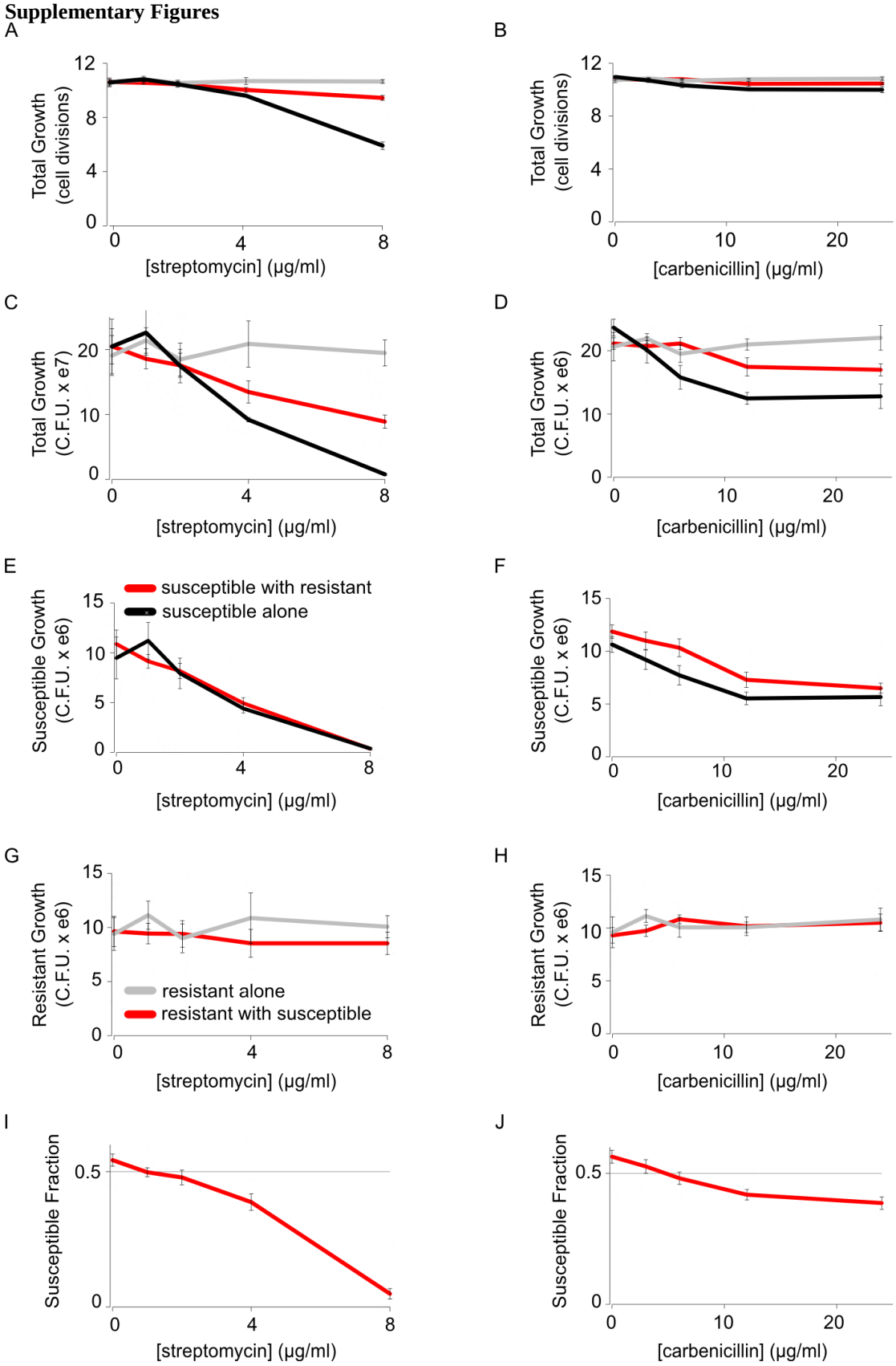

Figure S1. Cell count data from the liquid culture experiment to supplement Figure 1, where we present these data in terms of cell divisions and fitness. Susceptible and resistant strains were competed in liquid culture overnight, with either carbenicillin (extracellular resistance) or streptomycin (intracellular resistance). At all concentrations tested, there is never an increase in selection for the susceptible strain, in the presence of the antibiotic. Final susceptible, resistant and total cell counts and

total growth rates are shown for streptomycin (A, C, E, G) and carbenicillin (B, D, F, H). The final susceptible fraction has also been calculated in streptomycin (I) and carbenicillin (J). The mean and standard error of two experiments, each with n = 6 for co-cultures and n = 3 for monocultures, are shown.

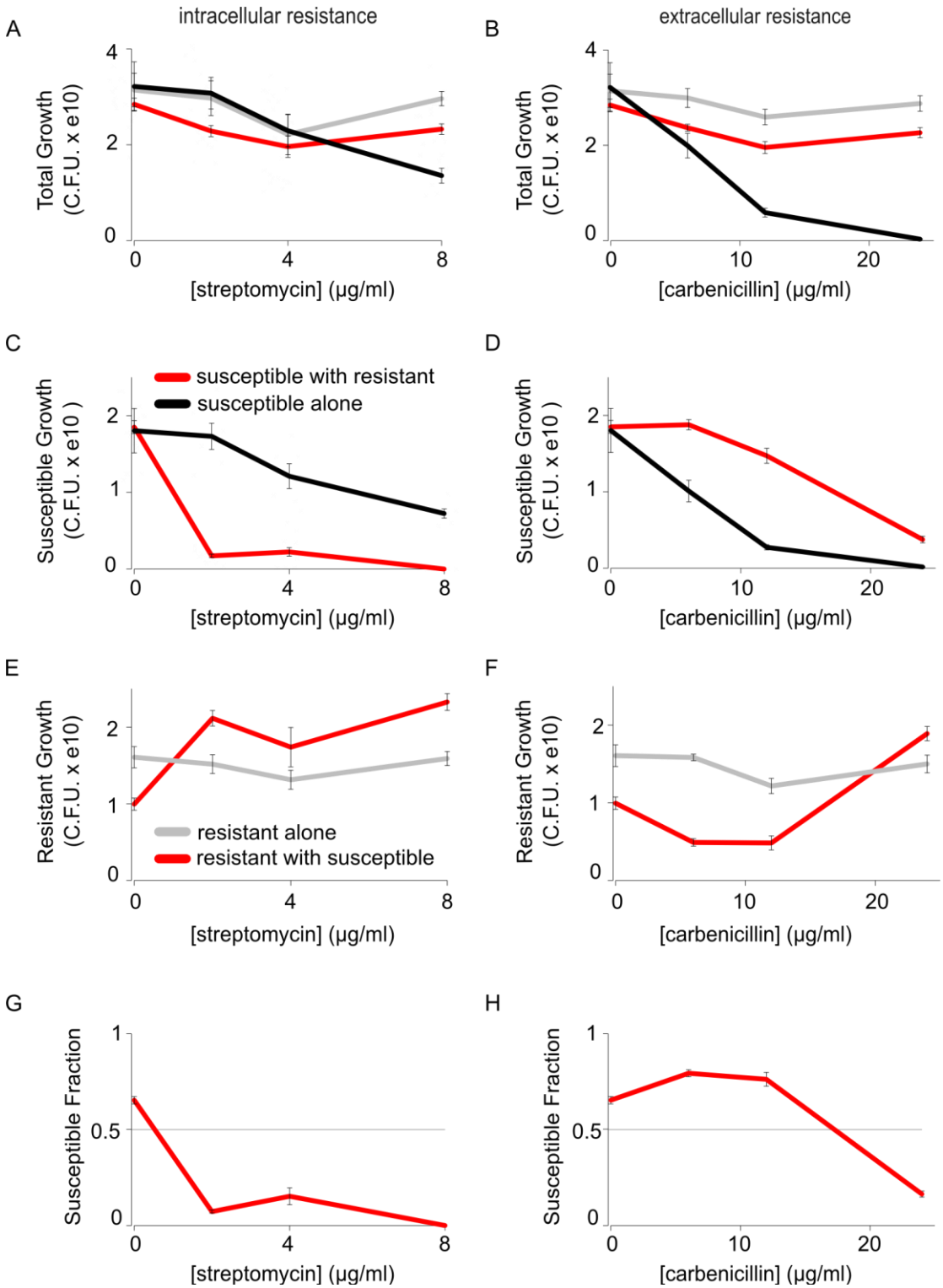

Figure S2. Cell count data from growth on agar experiment to supplement Figure 2, where we present these data in terms of cell divisions and fitness. During growth on agar, in the presence of streptomycin (intracellular resistance) there is always selection for the resistant strain (A, C, E, G). However, when the resistance mechanism is extracellular, as is the case for carbenicillin, there is selection for the susceptible strain (B, D, F, H). The mean and standard error of two experiments, each with n = 6 for co-cultures and n = 3 for monocultures, are shown.

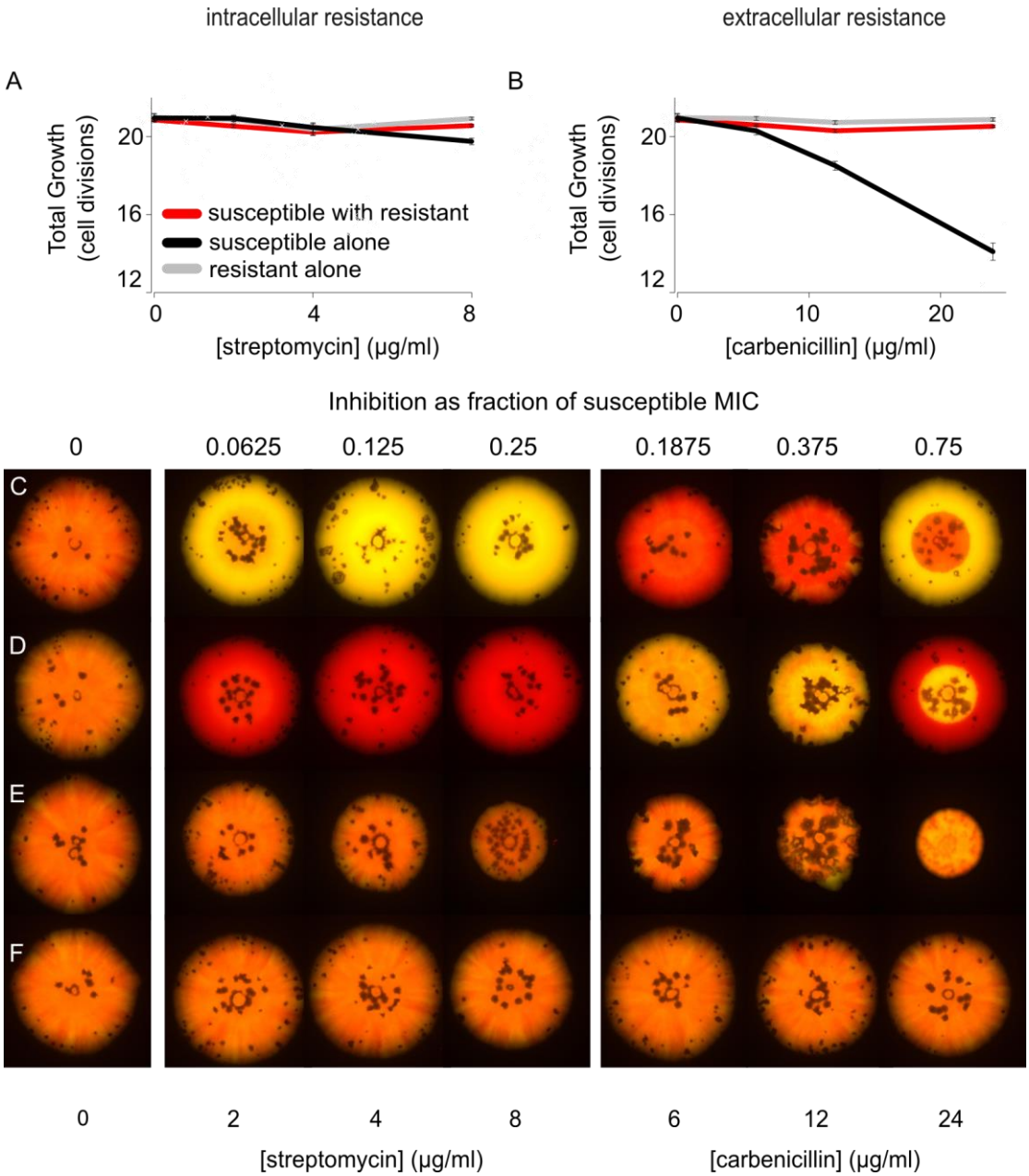

Figure S3. Total growth rate and accompanying colony images of competitions on agar to supplement Figure 2, where we present these data in terms of susceptible and resistant growth and show only the colony images for competitions between susceptible and resistant strains. During growth on agar in the presence of streptomycin (intracellular resistance) there is always selection for the resistant strain. However, when the resistance mechanism is extracellular, as is the case for carbenicillin, there is selection for the susceptible strain at intermediate concentrations. Total growth rates are shown on streptomycin (A) and carbenicillin (B). Images of the following competitions after 6 days of growth are shown: yellow resistant and red susceptible (C), yellow susceptible and red resistant (D), both colour susceptible (E) and both colours resistant (F). The mean and standard error of two experiments, each with n = 6 for co-cultures and n = 3 for monocultures, are shown.

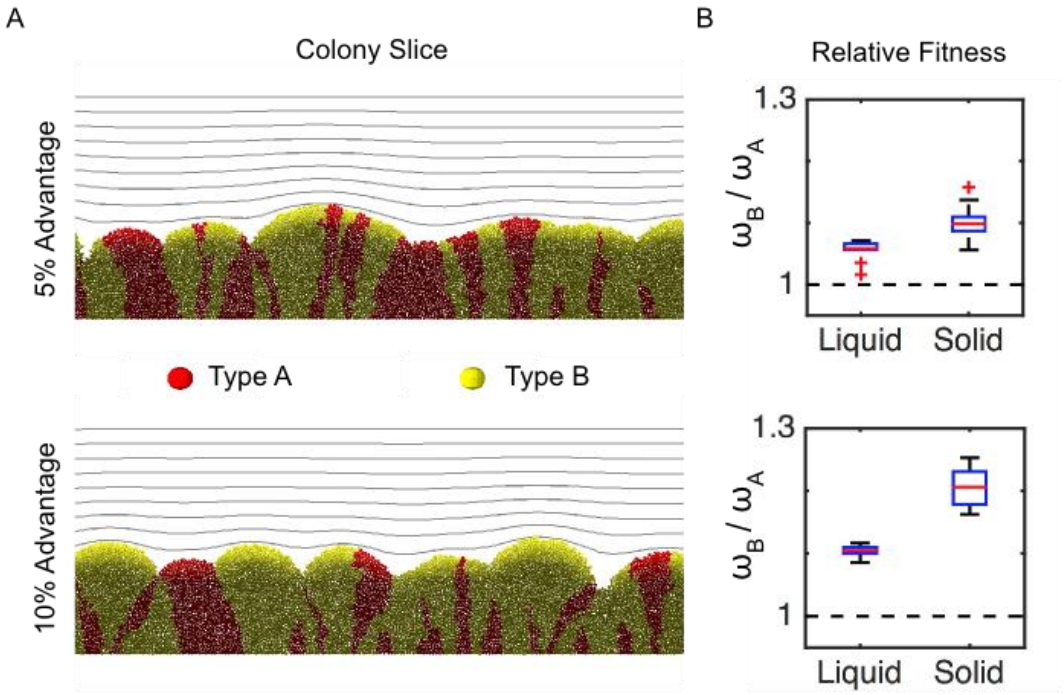

Figure S4. Individual-based modelling demonstrates that solid culture conditions can amplify cell growth advantages. We modelled competitions between identical cell shapes A and B (pictured centre), conferring B cells with either a 5% (top row) or 10% (bottom row) growth rate advantage over A-type cells. Representative screenshots (A) show 2D colony sections grown under solid culture conditions, where rapid cell growth is limited to a thin layer at the top of the colony. Cells are coloured by type and by growth rate as previously (Figure 6), so that fast-growing cells appear brightly-coloured. Contours correspond to Oxygen concentration isoclines in increments of 10% of $u_{O,0}$; snapshots show the central 200 µm section of the simulation domain. Plots of relative cell fitness ω_B / ω_A, show that the type-B cell growth rate advantage is increased approximately 2-fold, under solid culture conditions relative to liquid culture controls, in which the entire colony receives sufficient perfusion for rapid growth (B). 10 simulation replicates were sampled per case.

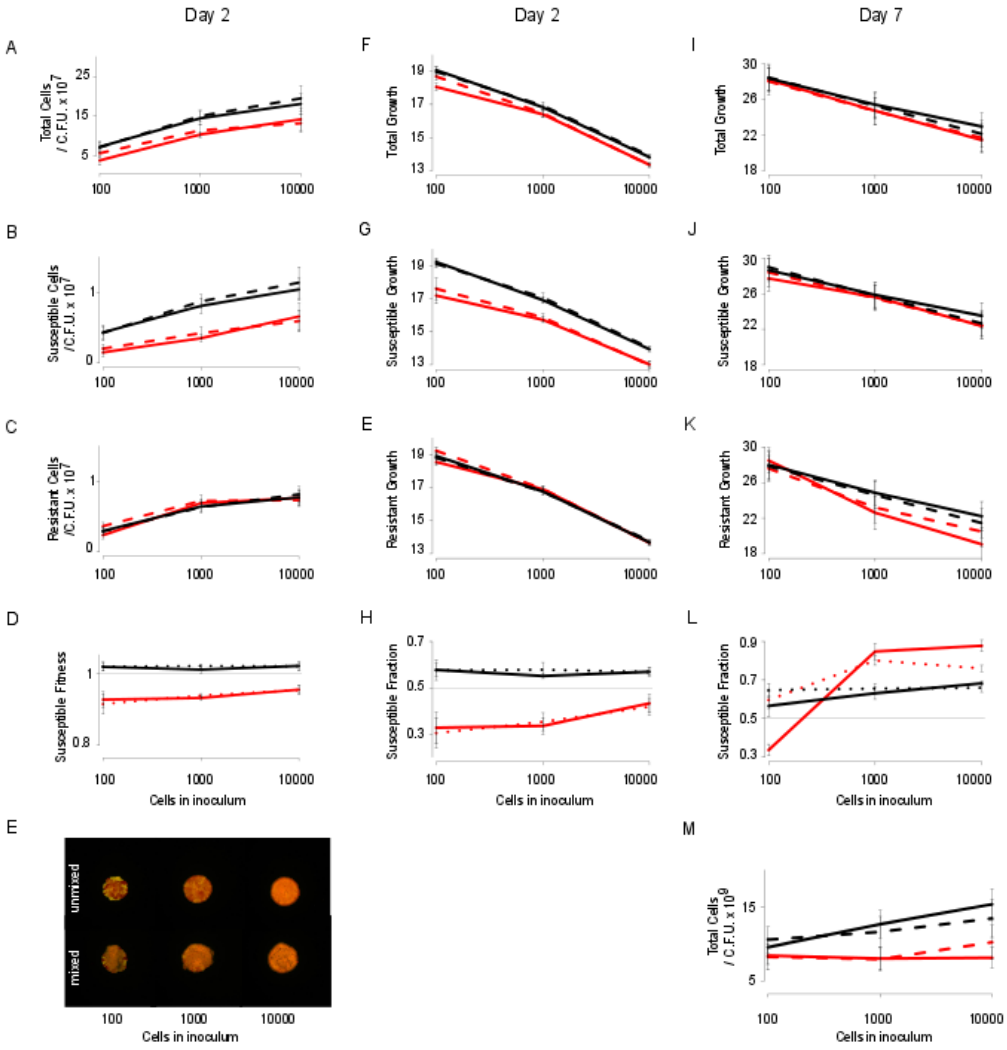

Figure S5. 2 day and 7 day growth with increasing inoculum density to supplement Figure 4, where we present only the 7 day growth in terms of cell divisions and fitness. Susceptible and resistant strains were co-inoculated onto plates containing either no antibiotic (black line) or 12 µg/ml carbenicillin (red line). The dotted line shows a mixing treatment used to disrupt any emergent spatial structure. After two days, before colonies are confluent, mixing has no effect on growth (A, B, C, D, E, G, F, G, H). However after 7 days, when spatial structure has been allowed to develop, mixing restores selection for susceptible strains in the most highly structured (lowest inoculum) density colonies (I, J, K, L, M). This is not the case when there is no antibiotic present. The mean and standard error of two experiments, each with n = 3, are shown.

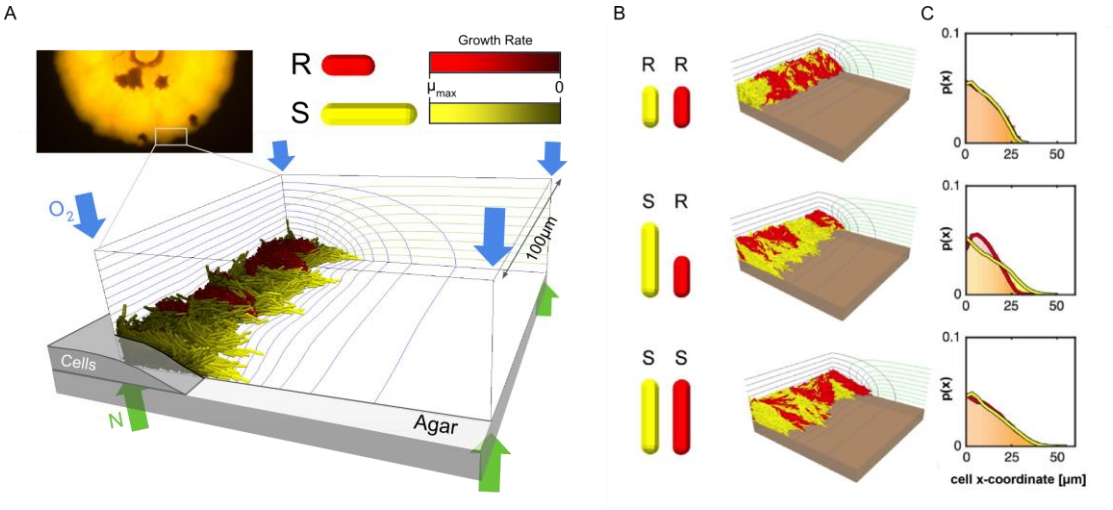

Figure S6. Simulating growth at the colony edge using a 3D hybrid individual-based model shows cell morphology drives the fitness advantage of susceptible cells. This is a supplement to Figure 6, where we present the results of this model. We use a hybrid modelling framework (A) to simulate resource competition between different cell shapes. A 100 μm section of the colony edge is modelled using a walled cuboidal domain, containing both discrete cells and continuous chemical fields. Resistant (R) or susceptible (S) cells are represented using short or long capsules, respectively. Cells elongate according to the local concentration of Oxygen (O_2, blue contours) and Nutrient (N, green contours), which diffuse into the colony from above and below as indicated. Each cell is coloured by its individual growth rate: both resources are required for growth such that only cells on the outer edge of the colony are able to proliferate. Repulsive elastic forces between growing capsules lead to expansion of the colony edge along the agar surface. Contours mark isoclines in each field in increments of 10%. The 3D colony edge simulations produced by this model show cell morphology drives the fitness advantage of antibiotic-susceptible (S) cells (B, C). Mixtures of cells with short resistant (R) and long susceptible (S) aspect ratios (SR) behave differently to control simulations where both strains have the same shape (RR, SS) (B). The S cell is more sensitive to branching, leading to enrichment at the colony edge when grown alongside R cells. This does not occur in the RR case, in which neither strain branches, nor the SS case, in which both strains branch. Histograms of cell x-coordinate quantify the enrichment of S cells at the colony edge in the SR case only (C). The spatial structure produces a growth rate advantage for S cells in SR mixtures, but not otherwise. All data were taken after 56 hours of growth, using a merged sample of 10 colonies.

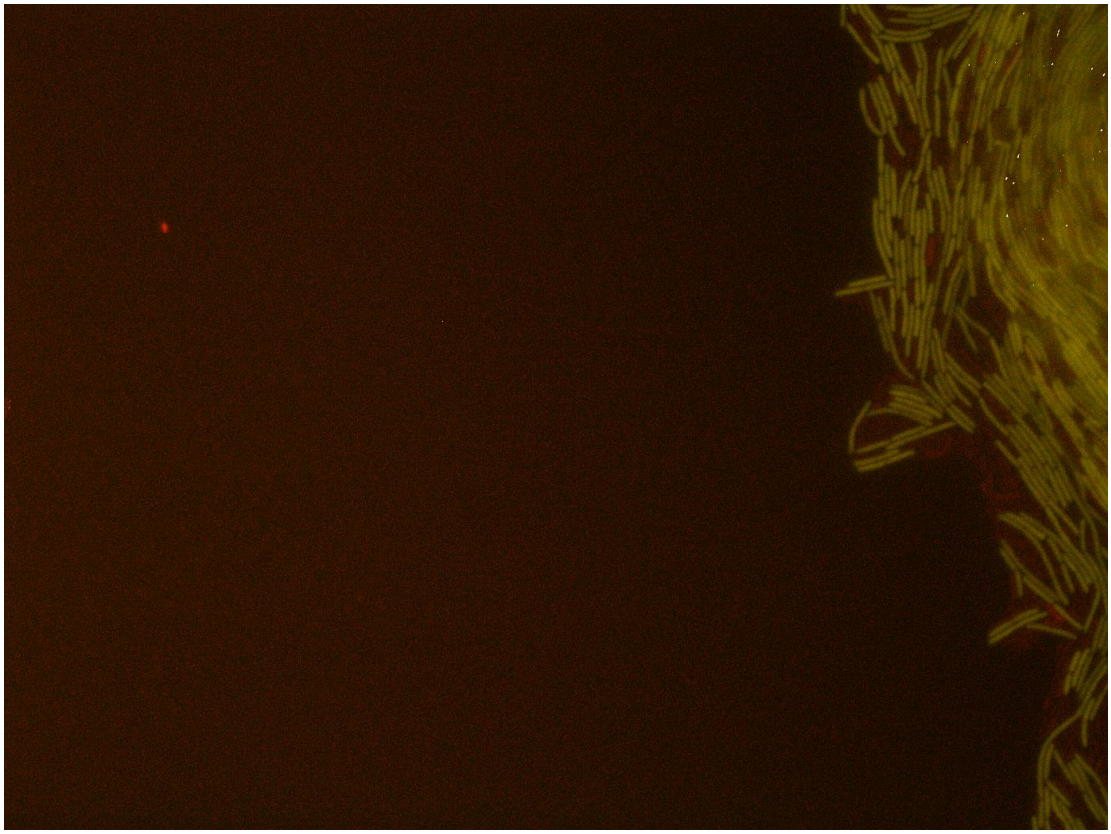

Movie S1. Time-lapse images show longer susceptible cells extend from the colony edge and occlude the shorter resistant cells. This data is presented as a supplement to the micrograph images in Figure 6, where we present images from a short portion of this movie. Movie of growth at the colony edge after 10 hours on 12 μg/ml carbenicillin, with frames taken every minute. Susceptible strains are imaged in yellow and resistant strains in red.

Supplementary Tables

	Carbenicillin (μg/ml)		Streptomycin (μg/ml)	
Strain	LB broth	LB agar	LB broth	LB agar
Resistant	8192	8192	2048	2048
Susceptible	32	32	16	32

Table S1. Minimum inhibitory concentration (MIC) of streptomycin and carbenicillin to plasmid-(Rms149) bearing resistant strain and plasmid-free susceptible strain, when grown on solid and liquid LB media.

	MSC (μg/ml) as fraction of susceptible MIC	
Antibiotic	*Agar*	*Broth*
Carbenicillin	20 (0.62 MIC)	2.3 (0.071 MIC)
Streptomycin	0.78 (0.024 MIC)	1.6 (0.097 MIC)

Table S2. Minimum Selective Concentration (MSC) was calculated by fitting susceptible fitness data from competition experiments to a quadratic model. These calculations are described in greater detail in the Supplementary Experimental Procedures.

Supplementary Experimental Procedures

Rms149-F	GCCGTATTTCATCAACAT
Rms149-R	ACGAAGCTGAAGATTTAC

Primers used in this study (15)**.**

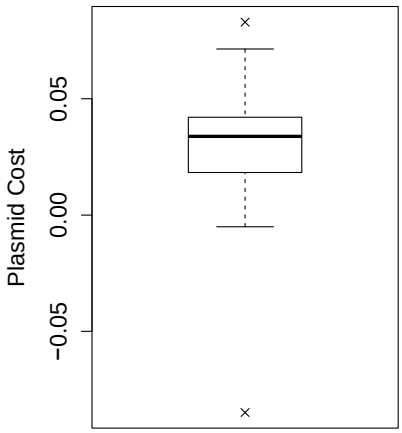

Plasmid cost without antibiotic. Flow cytometry was used to calculate the cost of Rms149 plasmid carriage without antibiotic in liquid culture. The fitness cost was found to be 3 % (s.e. = 0.38 %) n = 46.

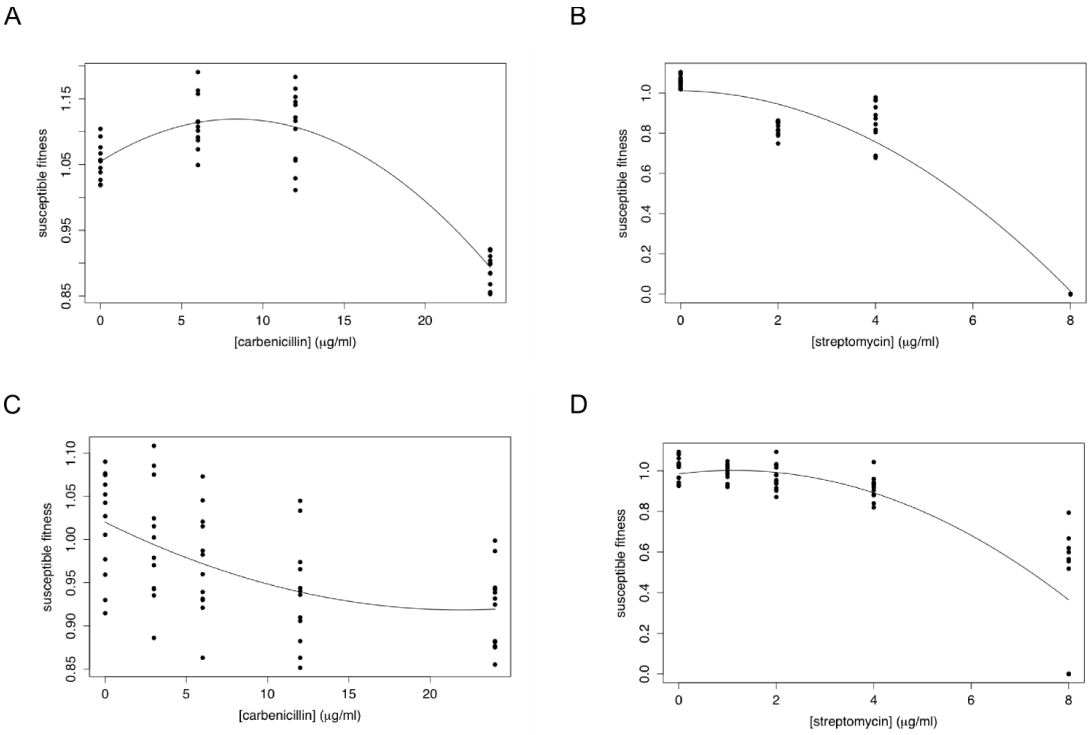

To estimate the minimum selective concentration (MSC) quadratic models were fitted to the fitness of the susceptible strain relative to the resistant strain in the four cases of colony growth on carbenicillin (A) or streptomycin (B) and liquid growth on carbenicillin (C) or streptomycin (D). The coefficients from these models are outlined below.

Coefficients:	Estimate	Std. Error	Pr(>|t|)
(Intercept)	1.055e+00	1.064e-02	< 2e-16 ***
concentration	1.543e-02	2.252e-03	1.69e-08 ***
concentration^2	-9.232e-04	8.703e-05	7.94e-14 ***

Multiple R-squared: 0.8508, Adjusted R-squared: 0.8442
P-value: < 2.2e-16
A quadratic model was fitted to the fitness of the susceptible strain growing as a colony on carbenicillin.

Coefficients:	Estimate	Std. Error	Pr(>|t|)
(Intercept)	1.0200949	0.0143083	< 2e-16 ***
concentration	-0.0092886	0.0033783	0.00798 **
concentration^2	0.0002121	0.0001317	0.11279

Multiple R-squared: 0.2904, Adjusted R-squared: 0.2655
P-value: 5.669e-05
A quadratic model was fitted to the fitness of the susceptible strain growing in liquid containing carbencillin.

Coefficients:	Estimate	Std. Error	Pr(>|t|)
(Intercept)	1.011371	0.027196	< 2e-16 ***
concentration	-0.002723	0.017261	0.875
concentration^2	-0.015237	0.002001	1.26e-09 ***

Multiple R-squared: 0.9455, Adjusted R-squared: 0.9431
P-value: < 2.2e-16
A quadratic model was fitted to the fitness of the susceptible strain growing as a colony on streptomycin.

Coefficients:	Estimate	Std. Error	Pr(>|t|)
(Intercept)	0.984739	0.037451	< 2e-16 ***
concentration	0.030807	0.026527	0.25
concentration^2	-0.013542	0.003103	5.42e-05 ***

Multiple R-squared: 0.73, Adjusted R-squared: 0.7205
P-value: < 2.2e-16
A quadratic model was fitted to the fitness of the susceptible strain growing in liquid containing streptomycin.

Supplementary Experimental Procedures relating to the model

Variables used in this study.

Variable	Symbol	Units
Cartesian coordinates	x, y, z	m
Cell volume fraction field	$\varphi(p_1 \ldots p_n)$,	-
Oxygen field	u_O	kg m^{-3}
Nutrient field	u_N	kg m^{-3}
For each cell i:		
position vector	$p_i = (p_x, p_y, p_z)_i^{\mathsf{T}}$	m
orientation unit vector	$\hat{a}_i = (a_x, a_y, a_z)_i^{\mathsf{T}}$	-
segment length	l_i	m
volume	$V_i = \frac{4}{3}\pi R_i^3 + \pi l_i R_i^2$	m^3
local Oxygen concentration	$u_O(p_i)$	kg m^{-3}
local nutrient concentration	$u_N(p_i)$	kg m^{-3}
specific growth rate	$\mu_{max}\left(\frac{u_O(p_i)}{u_O(p_i) + K_O}\right)\left(\frac{u_N(p_i)}{u_N(p_i) + K_N}\right)$	s^{-1}

Model parameters used in this study. Units and sources listed apply to all parameters in groups (indicated with indentation in column 1), unless specified otherwise.

Parameter	Symbol	Value	Units	Source
Domain size:			m	(13)
width	L_x	0.1 x 10^{-3}		
depth	L_y	0.1 x 10^{-3}		
height	L_z	$\max(p_x) + \delta$		
Cell radius	r	0.5 x 10^{-6}	m	(11)
Cell birth aspect ratio:	AR_0		-	This study
R-type		2.5		
S-type		4.5		
Boundary height	δ	20.0 x 10^{-3}	m	(16)
Solute diffusivity:			m^2s^{-1}	
Oxygen	D_O	2.0 x 10^{-9}		(13)
Nutrient	D_N	1.0 x 10^{-9}		
Bulk concentrations:			kg m^{-3}	
Oxygen	$u_{O,bulk}$	0.5 x 10^{-3}		(13)
Nutrient	$u_{N,bulk}$	0.25 x 10^{-3}		Assumed
Cell biomass density	ρ	290	kg m^{-3}	(13)
Max. specific uptake rate	μ_{max}	15.2 x 10^{-6}	s^{-1}	(13)
Saturation constant:			kg m^{-3}	
Oxygen	K_O	0.17 x 10^{-3}		(16)
Nutrient	K_N	0.85 x 10^{-3}		Assumed
Biomass yield:			-	
Oxygen	γ_O	22.22		(13)
Nutrient	γ_N	55.55		Assumed
FEniCS solver tolerance	ε_F	1.0 x 10^{-6}	-	(16)
Mesh element length	h_F	5.0 x 10^{-6}	m	(16)
Division axis noise	ξ_{ax}	9	%	(11)
Division volume noise	ξ_{div}	0.2	%	(11)
Regularisation weight	α	0.04	-	(11)
CM solver tolerance	ε_{CM}	1.0 x 10^{-3}	-	(11)
Number of substeps	N_{sub}	10	-	(11)
Max. contact iterations	N_{iter}	8	-	(11)
Cell grid element length	h_{CM}	10.0 x 10^{-6}	m	(11)
Time step	Δt	2.0	h	This study

Solute PDE boundary conditions used in this study.
$\hat{n}$ refers to the unit vector tangential to a given domain boundary.

Solute	Boundary	Condition	Description
Oxygen (O)	Top	$u_O = u_{O,bulk}$	Supply from bulk fluid
	Base	$\nabla u_O \cdot \hat{n} = 0$	Zero flux through agar
	Sides	$\nabla u_O \cdot \hat{n} = 0$	Zero flux through sides
Nutrient (N)	Top	$u_N = 0$	Removal by bulk fluid
	Base	$u_N = u_{N,bulk}$	Supply from agar
	Sides	$\nabla u_N \cdot \hat{n} = 0$	Zero flux through sides

Supplementary References

1. Suh S-J, Silo-Suh L a, Ohman DE (2004) Development of tools for the genetic manipulation of *Pseudomonas aeruginosa*. *J Microbiol Methods* 58(2):203–12.
2. Haines AS, Jones K, Cheung M, Thomas CM (2005) The IncP-6 plasmid Rms149 consists of a small mobilizable backbone with multiple large insertions. *J Bacteriol* 187(14):4728–4738.
3. Choi KH, Schweizer HP (2006) Mini-Tn7 insertion in bacteria with single attTn7 sites: example *Pseudomonas aeruginosa*. *Nat Protoc* 1(1):153–61.
4. Wiegand I, Hilpert K, Hancock REW (2008) Agar and broth dilution methods to determine the minimal inhibitory concentration (MIC) of antimicrobial substances. *Nat Protoc* 3(2):163–75.
5. San Millan A, *et al.* (2014) Positive selection and compensatory adaptation interact to stabilize non-transmissible plasmids. *Nat Commun* 5:5208.
6. Lenski RE, Rose MR, Simpson SC, Tadler SC (1991) Long-Term Experimental Evolution in *Escherichia coli*. I. Adaptation and Divergence During 2,000 Generations. *Am Nat* 138(6):1315–1341.
7. van Gestel J, Weissing FJ, Kuipers OP, Kovács AT (2014) Density of founder cells affects spatial pattern formation and cooperation in *Bacillus subtilis* biofilms. *ISME J* 10(8):2069–2079.
8. Kim W, Racimo F, Schluter J, Levy SB, Foster KR (2014) Importance of positioning for microbial evolution. *PNAS* 111(16):E1639–E1647.
9. Schindelin J, *et al.* (2012) Fiji: an open-source platform for biological-image analysis. *Nat Methods* 9(7):676–82.
10. RStudio (2012) RStudio. Available at: http://www.rstudio.org/.
11. Rudge TJ, Steiner PJ, Phillips A, Haseloff J (2012) Computational modeling of synthetic microbial biofilms. *ACS Synth Biol* 1(8):345–352.
12. Rudge TJ, Federici F, Steiner PJ, Kan A, Haseloff J (2013) Cell polarity-driven instability generates self-organized, fractal patterning of cell layers. *ACS Synth Biol* 2(12):705–714.
13. Picioreanu C, Van Loosdrecht MCM, Heijnen JJ (1998) Mathematical modeling of biofilm structure with a hybrid differential- discrete cellular automaton approach. *Biotechnol Bioeng* 58(1):101–116.
14. Nadell CD, Foster KR, Xavier JB (2010) Emergence of spatial structure in cell groups and the evolution of cooperation. *PLoS Comput Biol* 6(3):e1000716.
15. San Millan A, Heilbron K, MacLean RC (2014) Positive epistasis between co-infecting plasmids promotes plasmid survival in bacterial populations. *ISME J* 8(3):601–12.
16. Smith WPJ, *et al.* (2016) Cell morphology drives spatial patterning in microbial communities. *PNAS*.